Applied Catalysis B: Environmental 125 (2012) 180–188

Contents lists available at SciVerse ScienceDirect

Applied Catalysis B: Environmental

journal homepage: www.elsevier.com/locate/apcatb

General strategy for one-pot synthesis of metal sulfide hollow spheres with enhanced photocatalytic activity

Man Luo [a], Yong Liu [a], Juncheng Hu [a,*], Jinlin Li [a], Jun Liu [b], Ryan M. Richards [c]

[a] Key Laboratory of Catalysis and Materials Science of the State Ethnic Affairs Commission & Ministry of Education, South-Central University for Nationalities, Wuhan 430074, PR China
[b] Pacific Northwest National Laboratory, Richland, WA 99352, USA
[c] Department of Chemistry and Geochemistry, Colorado School of Mines, Golden, CO 80401, USA

ARTICLE INFO

Article history:
Received 19 March 2012
Received in revised form 18 May 2012
Accepted 27 May 2012
Available online 4 June 2012

Keywords:
Hollow spheres
Metal sulfide
CdS
ZnS
Photocatalysis

ABSTRACT

A gas bubble-templating method has enabled synthesis of a diverse portfolio of hollow transition-metal sulfides microspheres (e.g., CdS, ZnS, CuS and Bi_2S_3) by a general one-step route. The products were characterized by X-ray powder diffraction, scanning and transmission electron microscopy, high-resolution transmission electron microscopy, energy dispersive spectroscopy analysis, N_2 adsorption and UV–vis diffuse reflectance spectroscopy. The shell of all hollow spheres is composed of single-crystal metal sulfide nanoparticles and the shell thickness can be readily controlled by changing the deposition time. These hollow microspheres are envisioned to have broad applications in catalysis, Li-ion batteries, microreactors, biomedicines, etc. As an example, here, we demonstrate that the prepared CdS and ZnS hollow sub-micrometer spheres are excellent photocatalysts with higher photodegradation efficiency of potential polluting agents than that of commercial CdS, ZnS and TiO_2 P25 under visible light and UV light illumination, respectively.

1. Introduction

Hollow structured micro- or nanoscopic materials have recently attracted special attention due to their superior properties such as lower density, higher specific surface area, similarity to cells and membranes, and better permeability compared to their solid counterparts [1–8]. These outstanding properties make them promising for a series of applications such as drug-delivery systems [9,10], lithium-ion batteries [5,11–13], and catalysts [14–16]. To present, various hollow spheres including carbons, polymers, metals and inorganic materials have been extensively investigated. Transitional metal sulfide hollow spheres are of particular interest for potential applications in the field of optics, electronics, and optoelectronics [17–19].

Traditionally, template-directed methods have included hard templates (e.g., silica spheres, carbon spheres, and metal nanoparticles) [1,5,7,8,14,20,21] and soft templates (e.g., micelles, emulsion droplets, liquid drops, and even bacteria) [22–26] to prepare micro- or nano-sized hollow spheres. However, the following inherent drawbacks greatly restricted their practical application: (i) these template-assisted methods often suffer from difficulty of coating the desirable materials on the template surface due to materials incompatibility issues, thus they are often only suitable for very specific applications; (ii) these template-assisted methods often require large quantities of surfactants and involve tedious operational procedures related to the repeated application of coatings and final removal of the templates; (iii) if the sacrificial template is removed by calcinations or solvent extraction, collapse and high non-uniformity of some fraction of the hollow structures is very likely. Therefore, developing a facile, economic and general synthesis strategy for one-step synthesis of various hollow spheres with no additional core removal step is of great importance and still a major challenge for material scientists.

The in situ gas-bubble template synthesis strategy [27–31] is a new method having the advantage of synthesizing hollow spheres in one-step approach, negating the template removal step in hollow material preparation which may effectively solve most of the above problems. As compared to the other template-synthetic methods, this new method is very simple, convenient and avoids the introduction of impurities. For example, ZnSe hollow spheres were synthesized under hydrothermal conditions using hydrazine as the reducing agent, from which N_2 bubbles were generated and acted as soft template [32]. However, major unsolved challenges for gas-bubble templated methods is improving reproducibility, gaining control of tuning chemical composition, and controlling the interior architecture by a general procedure.

Hierarchical hollow materials are most commonly prepared by use of templates, the removal of which is typically done by

* Corresponding author. Tel.: +86 27 67841302.
E-mail address: junchenghuhu@hotmail.com (J. Hu).

0926-3373/$ – see front matter © 2012 Elsevier B.V. All rights reserved.
http://dx.doi.org/10.1016/j.apcatb.2012.05.041

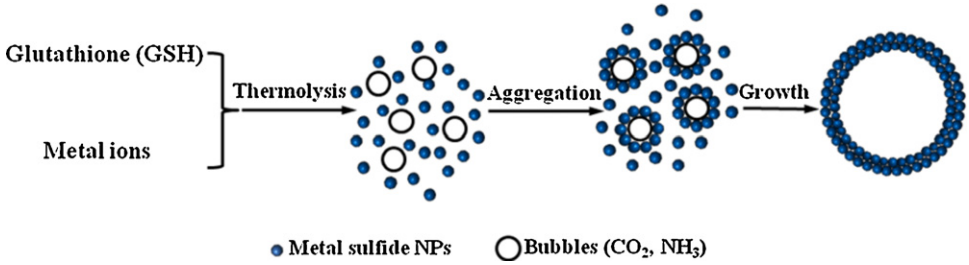

Scheme 1. Schematic illustration of the formation of the transition-metal sulfides hollow sub-micrometer spheres.

calcinations (or chemical etching) often leading to multi-step time-consuming procedures and often non-uniformity of the product. One approach towards more efficient non-sacrificial templating is to use gas bubbles. A gas bubble assisted method may open an exciting perspective for one-step synthesis of hollow materials owing to its efficient, economical and environmentally friendly characteristics. However, a key limitation of this technology thus far is its poor reproducibility and that the chemical composition of the final phase cannot be readily controlled. In this letter, we demonstrate a general one-pot synthesis of hollow sub-micrometer spheres of transition-metal sulfides as summarized in Scheme 1. In our synthesis route, the polypeptide glutathione (GSH), functions as a direct sulfur source for metal sulfide nanocrystal formation and also produces CO_2 and NH_3 bubbles during the reaction that are crucial to the formation of the hollow interiors. At an elevated temperature, the primary metal sulfide nanoparticles were formed by thermolysis of metal ions – GSH. Meanwhile, the gas bubbles of CO_2 and NH_3 were generated to provide the assembly centers during the reaction. Driven by the minimization of interfacial energy, the fresh-formed crystalline metal sulfide nanoparticles are unstable because of their high surface energy and they are thermodynamically favored to aggregate at the gas–liquid interface between the bubble and water [27–32]. A continuous aggregation process occurs at the gas–liquid interface and ultimately results in the formation of hollow metal sulfide spheres. Here, the energy (E) needed for the detachment of a nanoparticle from the bubble interface could be estimated as [33]:

$$E = \pi r^2 \gamma (1 - \cos\ \theta)^2 \quad (1)$$

where r is the radius of the nanoparticles, γ is the surface tension of the bubble interface, and θ is the contact angle of the liquid. Theoretical calculation shows that E is much larger than the thermal energy (the detailed calculation process is well described in Ref. [28]) of the nanoparticle, and thus these aggregated particles have little chance to escape from the bubble surface [28]. As an example, CdS, ZnS, CuS and Bi_2S_3 hollow spheres here were taken as model materials to demonstrate the strategy.

2. Experimental

2.1. Synthesis of metal sulfide hollow spheres

All chemicals were analytical grade (purchased from Aladdin) and were used as received without further purification. In a typical synthesis, 5.5 mmol $Cd(NO_3)_2$ and 5.5 mmol glutathione (GSH, $C_{10}H_{17}N_3O_6S$) were dissolved in 250 ml deionized water to form a clear solution after stirring for 30 min at room temperature. After transfer to an autoclave with an inner quartz sleeve, the autoclave was purged with nitrogen for 10 min to eliminate oxygen in the autoclave, and then a pressure of 10 bar nitrogen was introduced into the autoclave. The clear solution was heated to 200 °C and kept for 5–10 h, then allowed to cool to room temperature naturally. The obtained yellow CdS precipitate was washed with absolute acetone several times, and finally dried at 60 °C for 6 h in a vacuum. The same procedures are applied to synthesize ZnS, CuS and Bi_2S_3 hollow sphere samples when zinc nitrate, copper nitrate and bismuth nitrate was used as zinc source, copper source, and bismuth source, respectively.

2.2. Characterization

The crystalline structure of the catalysts was characterized by powder X-ray diffraction (XRD) employing a scanning rate of 0.05°/s in a 2θ range from 10° to 80°, in a Bruker D8 Advance using monochromatized Cu Kα radiation.

Scanning electron microscopy (SEM) was performed with a S4800 field emission SEM (FESEM, Hitachi, Japan) at an accelerating voltage of 5 kV. The SEM was linked to an Oxford Instruments X-ray analysis system.

The morphology and particle size of catalysts were analyzed by transmission electron microscopy using a Tecnai G20 (FEI) TEM operated at an accelerating voltage of 200 kV. HRTEM and electron diffraction data are collected using a FEI Titan TEM operated at 300 kV.

The UV–vis DRS were collected using a Shimadzu UV-2450 spectrophotometer from 200 to 800 nm using $BaSO_4$ as background.

The nitrogen adsorption measurements were done on a Micromeritics ASAP 2010 physisorption apparatus.

2.3. Photodegradation experiment

The photoactivity of the samples was tested by the degradation of Rhodamine B (50 ml, 1×10^{-5} mol L^{-1}) and salicylic acid (50 ml, 20 mg L^{-1}) under visible light (>420 nm) or near UV (365 nm) irradiation. In a typical experiment, 50 mg photocatalyst was suspended in RhB or salicylic acid solution, then the mixed solution was oscillated in darkness for 5 h. After reaching adsorption equilibrium, the photocatalytic reaction was initiated by irradiating the system with a 350 W Xenon lamp. At given time intervals, 4 ml aliquots were collected, centrifuged, and then filted to remove the catalyst particles for analysis. The filtrates were finally analyzed using a UV–vis spectrophotometer (UV-2450). For comparison, the photocatalytic activity of commercial CdS (or ZnS) powders (Aladdin reagent) and Degussa P25 were also tested at the same experimental conditions.

2.4. Analysis of hydroxyl radicals (•OH)

The production of •OH on the surface of vis-illuminated CdS hollow spheres was detected by a photoluminescence (PL) method using coumarin as a probe molecule. Coumarin can readily react with •OH to produce highly fluorescent product, 7-hydroxycoumarin (7HC) (umbelliferone) (see Scheme S1 in Supporting information). Experimental procedure was similar to the measurement of photocatalytic activity. In a typical process, CdS hollow spheres (50 mg) and coumarins (50 ml, 5×10^{-4} mol L^{-1}) were mixed under magnetic stirring for 4 h under dark conditions.

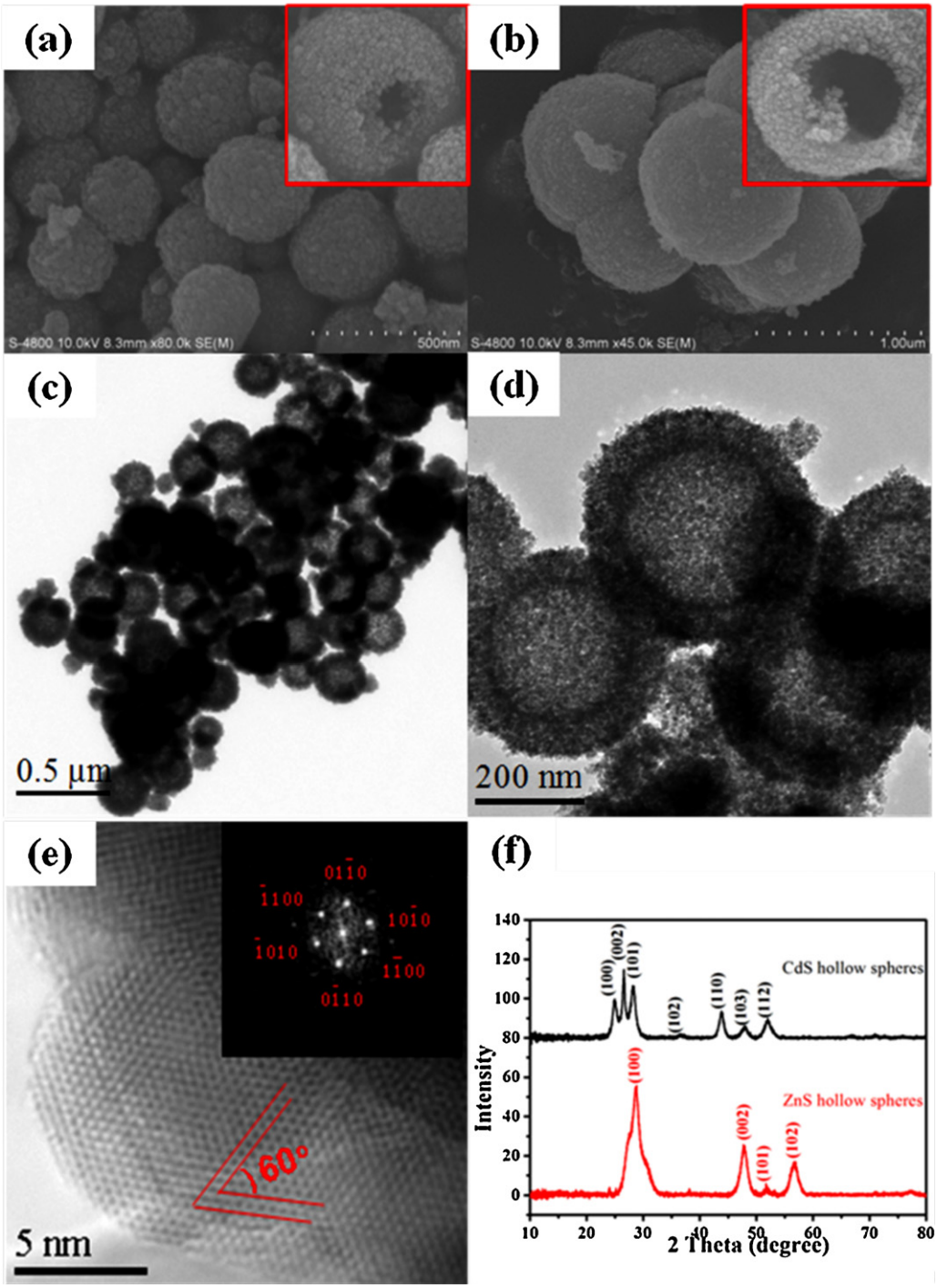

Fig. 1. FESEM images of the (a) hollow CdS spheres and (b) hollow ZnS spheres obtained at 200 °C for 5 h; TEM images of the (c) hollow CdS spheres and (d) hollow ZnS spheres obtained at 200 °C for 5 h; (e) HRTEM image of the shell region of a single CdS hollow sphere (the inset is two-dimensional fast Fourier transform pattern); (f) XRD patterns of CdS and ZnS hollow spheres.

Then, the mixture was irradiated under vis-light (>420 nm) light. After vis-light irradiation for 35 min, the reaction solution was filtrated to measure the increase in the PL intensity around 445 nm excited by 332 nm light.

3. Results and discussion

Fig. 1a and 1 are field-emission scanning electron microscopy (FESEM) images from which numerous spheres with an average diameter of about 350–400 nm for CdS (Fig. 1a) and 500–800 nm for ZnS (Fig. 1b) can be clearly observed. No other morphologies were observed, indicating a high yield of the product with hollow spherical morphology. Moreover, it is obvious that the surface of the sphere is coarse and the shells of the hollow spheres are constructed from fine nanoparticles (NPs). The NPs with diameter of 5–20 nm, as building blocks for the hollow spheres, can be further clearly observed on the wall of the broken hollow sphere (inset of Fig. 1a and b). It is interesting to note that the aggregation of these NPs can produce inherent porosity, which creates numerous nanoscale channels for chemical moieties travelling between the interior

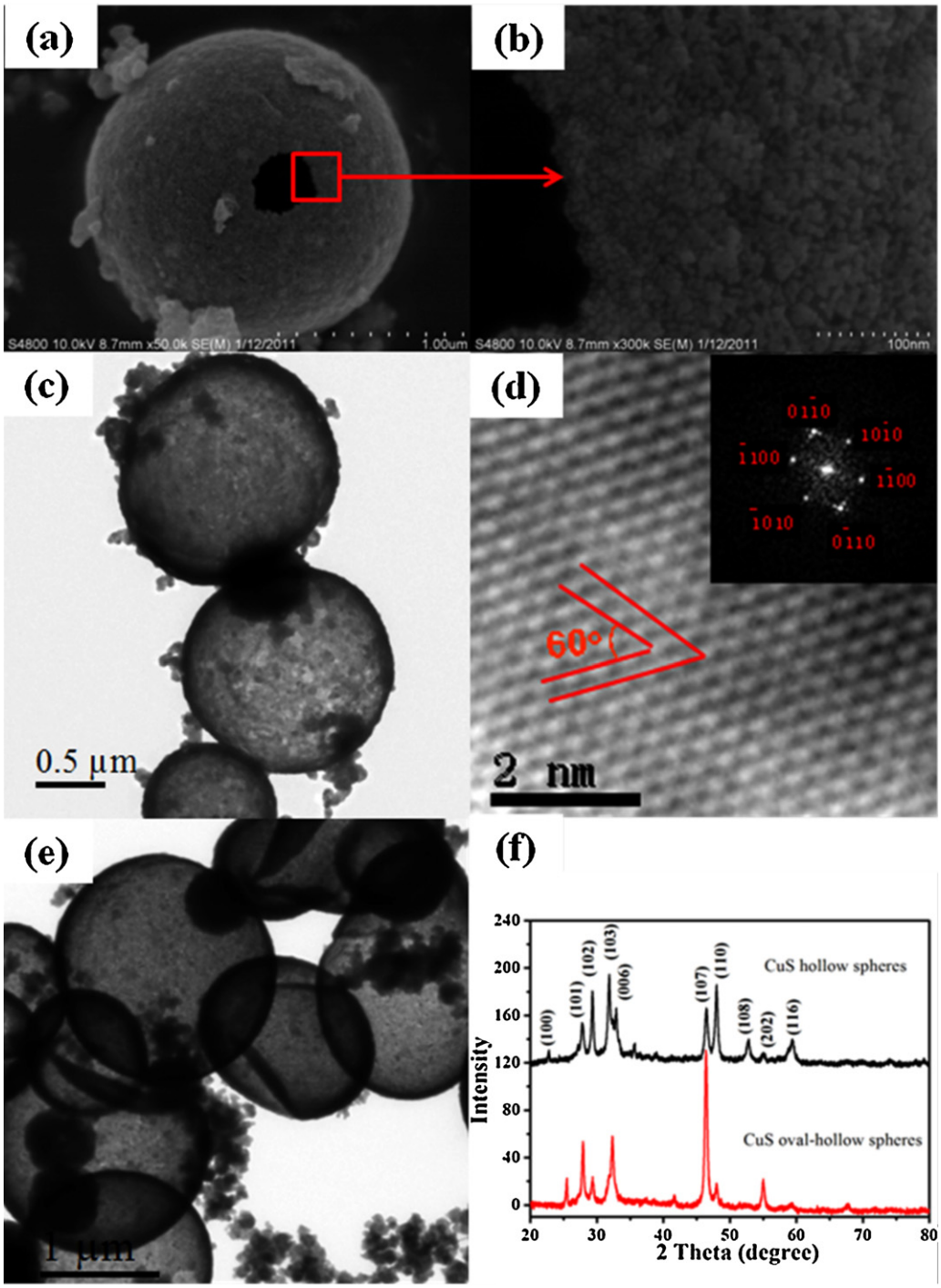

Fig. 2. (a) FESEM image of the hollow CuS spheres obtained at 180 °C for 5 h; (b) enlarged SEM image marked by red rectangle in (a); (c) TEM image of the hollow CuS spheres obtained at 180 °C for 5 h; (d) HRTEM image of the shell region of a single CuS hollow sphere (the inset is two-dimensional fast Fourier transform pattern); (e) TEM image of the oval-shaped CuS hollow spheres obtained at the ambient pressure exceeds 20 bar; (f) XRD patterns of CuS hollow spheres and oval-shaped CuS hollow spheres.

cavity and exterior space, thus making the hollow spheres particularly suitable for further studies in adsorption and catalytic applications. More detailed hollow structural features are revealed by TEM and HRTEM investigations. A clear contrast between the dark edge and the pale center can be observed, which confirms that all the spheres have a hollow interior (Fig. 1c and d). The hollow interiors have diameters of about 200 nm for CdS and 400 nm for ZnS hollow spheres, the thickness of the shell is estimated to be about 50 nm for CdS and 70 nm for ZnS hollow spheres, respectively. Fig. 1e is the typical high-resolution TEM (HRTEM) image of the shell region of a single CdS hollow sphere that displays the clear and continuous lattice planes, indicating the high crystallinity and single crystalline nature of the primary CdS NPs. The corresponding reciprocal lattice patterns obtained by two-dimensional fast Fourier transform of the lattice resolved images (inset of Fig. 1e), can be indexed to a wurtzite structure with a lattice constant $a = 4.1$ Å, which agrees well with previous studies of CdS nanowires [34].

The energy dispersive spectroscopy (EDS) analysis (Fig. S1 in Supporting Information) taken from SEM clearly

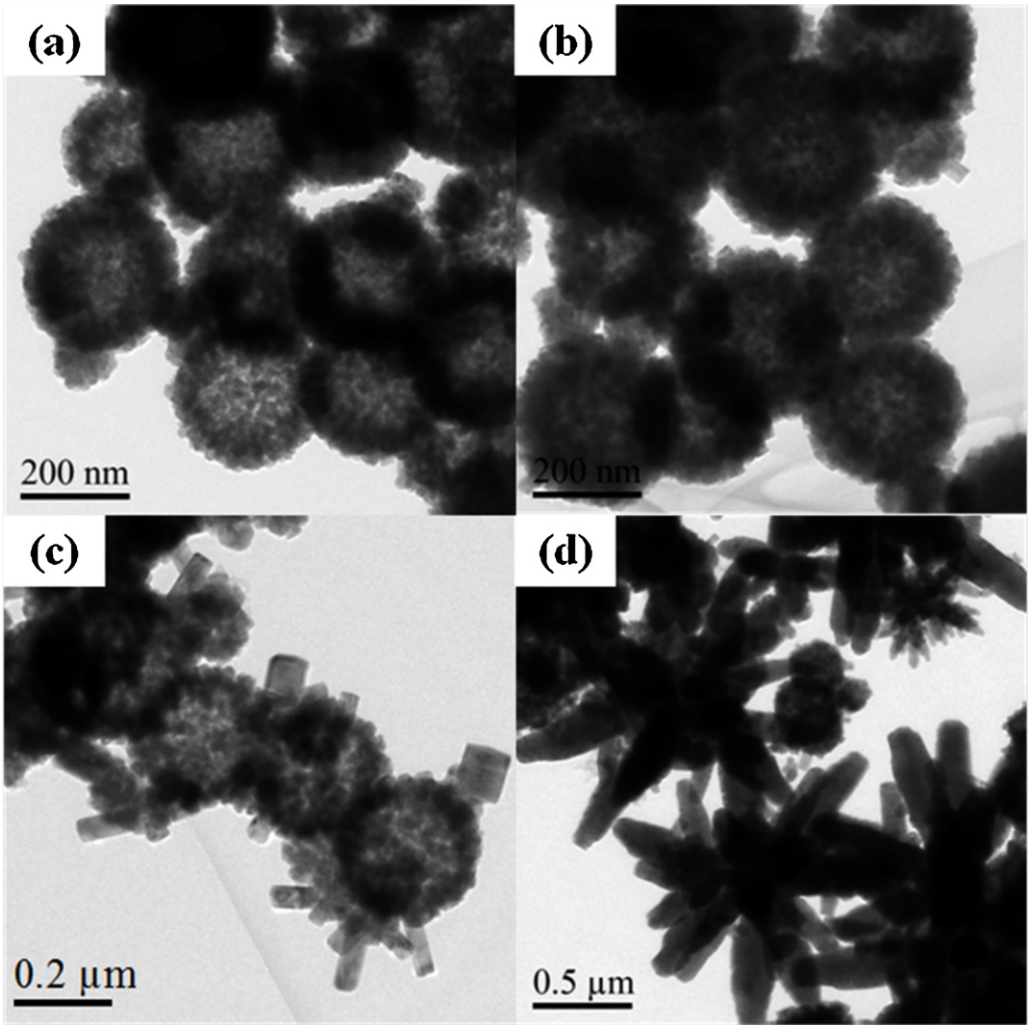

Fig. 3. TEM images of evolution for CdS hollow spheres at different reaction time: (a) 5 h, (b) 10 h, (c) 24 h, and (d) 50 h.

demonstrates that the molar ratio of Cd and S is 1.07:1 for CdS hollow spheres, and the Zn:S molar ratio is 1.02:1 for ZnS hollow spheres, close to that of the standard stoichiometric composition of the CdS and ZnS phases, respectively. The related X-ray diffraction (XRD) pattern of the hollow sphere samples is shown in Fig. 1f. All peaks of the as-prepared CdS can be assigned to the standard value of hexagonal CdS with lattice constants $a = 4.14$ Å and $b = 6.72$ Å (JCPDS no. 41-1049), which is consistent with the HRTEM result. Meanwhile, all peaks of the ZnS sample are in agreement with the standard data of the hexagonal wurtzite ZnS structure with lattice constants $a = 3.82$ Å and $b = 24.96$ Å (JCPDS no. 39-1363). No peaks are observed for impurities in any of the samples, indicating the high purity of the products.

To confirm the generality and validity of the proposed method, we have extended this facile and effective method to prepare a broad range of metal sulfide hollow spheres. Single-shelled hollow CuS sub-micrometer spheres have been obtained. The higher magnification FESEM image in Fig. 2a and b reveals its detailed nanostructure, in which the thickness of the shell of the CuS hollow sphere is estimated to be about 70 nm and the hollow sphere was also composed of aggregated CuS NP with sizes between 5 and 10 nm. TEM image in Fig. 2c shows that the single-shelled hollow CuS sub-micrometer spheres with an average diameter of about 1.5 μm. Obviously, the average size of the CuS hollow spheres is much larger than that of CdS (350–400 nm) and ZnS (500–800 nm) hollow spheres. This may relate to the different lifetime (T_e) of bubbles produced in the reaction system, since the lifetime of a bubble is directly proportional to its maximum radius, as given by the Rayleigh formula [35]:

$$T_e = 1.83\sqrt{\frac{\rho}{P - P_V}}R_{\max} \quad (2)$$

where ρ is the density of the liquid, P is the ambient pressure, P_V is the vapor pressure and $R_{\max}$ is the maximum radius of the bubble. The HRTEM image of a single CuS (Fig. 2d) exhibits clear lattice fringes, indicating high crystallinity of the CuS hollow spheres, and moreover, the reciprocal lattice patterns can be indexed to a wurtzite-structure (inset of Fig. 2d) with a lattice constant $a = 3.8$ Å.

More interestingly, we found that the surface morphology of the CuS hollow spheres can be well adjusted by varying the ambient pressure of the reaction system, which also infers that the formation of the hollow spheres on bubbles. As shown in Fig. 2e, the oval-shaped CuS hollow spheres can be obtained when the ambient pressure exceeds 20 bar. Here, we reasoned that the high ambient pressure may cause the collapse of the bubbles. After the collapse, the bubbles re-expand with a liquid flow, re-forming a distorted bubble, and thus provide aggregation centers to form oval-shaped hollow spheres [36]. Fig. 2f shows the XRD patterns of the CuS hollow spheres and oval-shaped CuS hollow spheres. It is seen that all the primary diffraction peaks of these two curves are in good agreement with the standard data for CuS (JCPDS no. 06-0464), which is

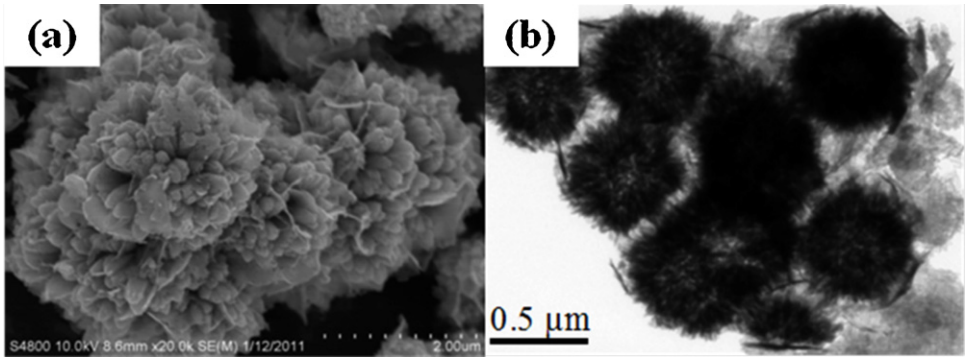

Fig. 4. (a) FESEM image and (b) TEM image of the hollow flowerlike Bi_2S_3 microspheres.

hexagonal structure (covellite, space group 194, $P6_3/mmc$), which is in agreement with the HRTEM results. The cell parameters of the products are $a = 3.784$ Å and $c = 16.331$ Å.

To better understand the evolution process of the hollow spheres, time-dependent experiments were carried out while fixing all other reaction parameters unchanged. Fig. 3a–d shows the detailed surface morphology of the CdS products obtained by varying reaction time. After the first reaction time of 5 h, the hollow CdS spheres with the shell thickness of about 50 nm were obtained by the aggregating of the crystalline nanoparticles around the gas/liquid interface between bubble and water (Fig. 3a). Upon increasing reaction time to 10 h, the continuous aggregation process occurs and the shell thickness is increased from 50 nm to 100 nm (Fig. 3b). Interestingly, when the reaction time is extended to 24 h, there is no apparent increase for the shell thickness with the increased reaction time, but there is a clear change in their surface morphology. As shown in Fig. 3c, the surface of the shell is covered with large amounts of nanorods, and these nanorods are perpendicular to the surface. And finally, when the reaction time was further prolonged to 50 h or longer, the flowerlike CdS crystalline with well-arranged nanorods are formed (Fig. 3d).

On the basis of the above evolution experiments, it is inferred that Ostwald ripening is likely the underlying mechanism for the formation of the flowerlike CdS crystalline (see Scheme 2). Ostwald ripening refers to the solution growth of larger crystals consuming smaller ones, which is a thermodynamically driven spontaneous process since a larger crystal is more energetically stable than a smaller one [37]. In this reaction, the tiny CdS nanoparticles first aggregated into hollow spheres. However, with the prolonged time, the loosely packed crystallites on the surface of the particles worked as nucleation points for the recrystallization process. Therefore, the aggregates will preferentially grow in one direction, forming the flowerlike morphology. Further experiments also lend support to the proposed evolution mechanism. As shown in Fig. 4, the hollow flowerlike Bi_2S_3 microspheres can be obtained when the reaction time was prolonged to 24 h. The high-magnification FESEM (Fig. 4a) clearly reveals that each bud in these hollow flowerlike microspheres is formed through assembly of many nanorods.

Generally, hollow transition metal sulfide materials can be widely used as drug-delivery systems, lithium-ion batteries, catalysts and so forth. Here, as an example of a potential application, the CdS hollow microsphere as-obtained was used as a photocatalyst in wastewater treatment. RhB, a common azo-dye in the textile industry, was chosen as a typical organic waste model. The installation of the photoreactor is shown in Fig. S2 (see the Supporting Information). Fig. 5 shows the change of absorption spectra of RhB aqueous solution (initial concentration is 1.0×10^{-5} M, 50 ml) in the presence of 50 mg CdS hollow spheres under visible light (>420 nm). The absorption peak at $\lambda = 553$ nm drops rapidly with increase of the exposure time and completely disappears after

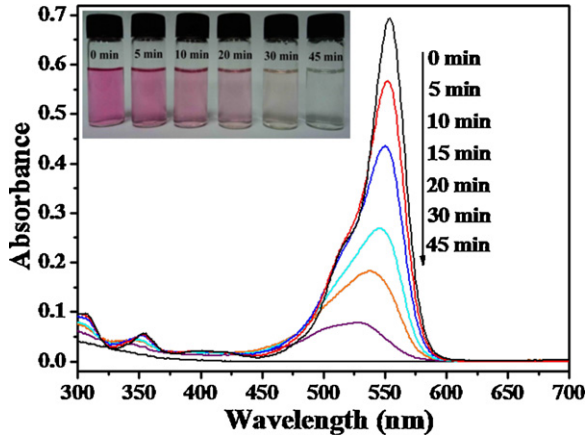

Fig. 5. The absorption spectrum of a solution of RhB (1.0×10^{-5} mol L^{-1}, 50 ml) in the presence of CdS hollow spheres (50 mg) under visible light (>420 nm) irradiation.

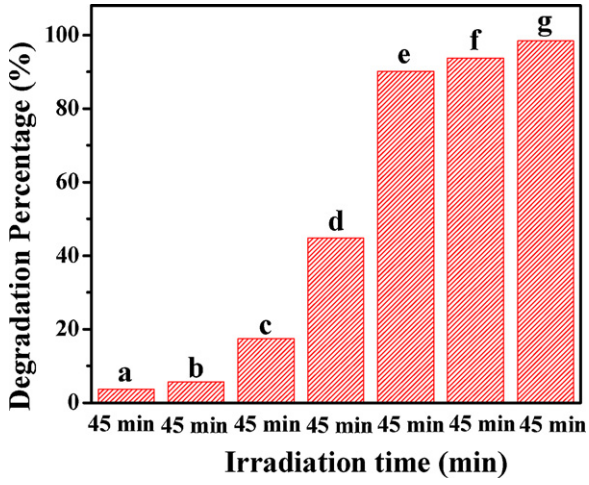

Fig. 6. Comparison of the photocatalytic activity of (a) catalyst free, (b) Degussa P25, (c) commercial CdS, (d) the flowerlike CdS crystalline, (e) CdS hollow spheres (200 °C, 24 h), (f) CdS hollow spheres (200 °C, 5 h) and (g) CdS hollow spheres (200 °C, 10 h) under visible light (>420 nm) irradiation.

45 min. No new absorption bands appear in either the visible or ultraviolet region indicating the complete photodegradation of RhB. For comparison, we also carried out decomposition of RhB dye in solution over the commercial CdS and Degussa P25 TiO_2 photocatalyst under visible light irradiation. The results are illustrated in Fig. 6. When the reactions were conducted without catalyst, only a slight decomposition (less than 5%) of RhB was detected under

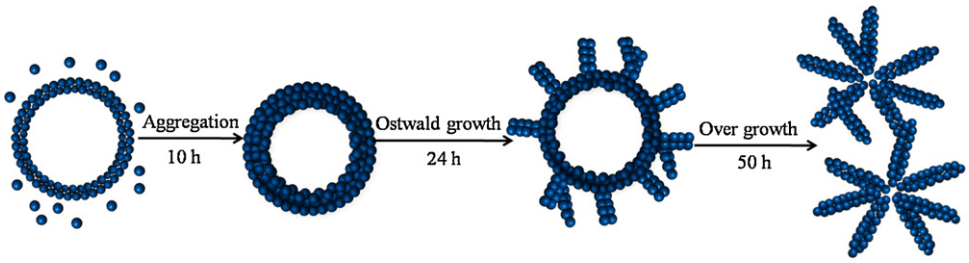

Scheme 2. Schematic illustration of the formation process of the flowerlike CdS crystalline.

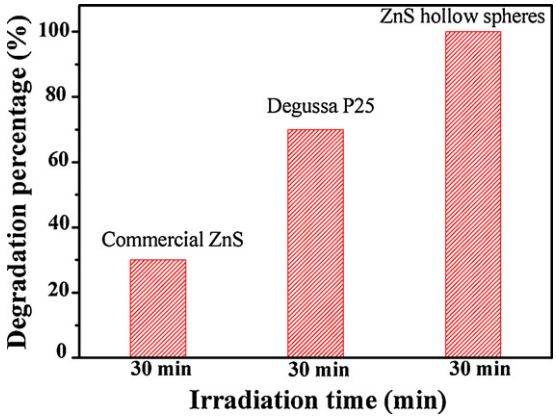

Fig. 7. Photocatalytic activity of (a) commercial ZnS, (b) Degussa P25 and (c) ZnS hollow spheres under UV light irradiation.

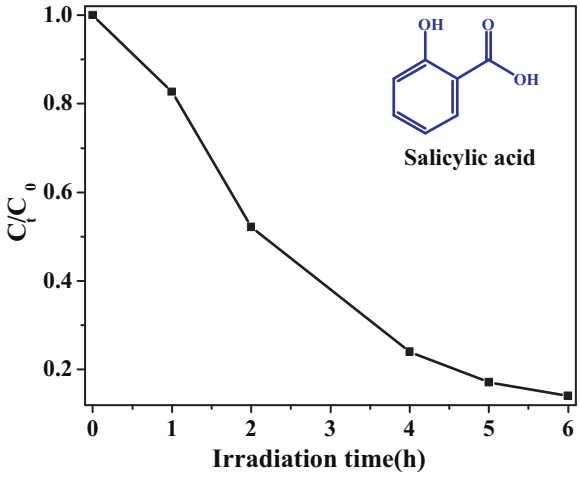

Fig. 8. C_t/C_0 versus time curves of salicylic acid photodegradation under visible light (>420 nm) irradiation over CdS hollow spheres.

visible light irradiation for 45 min (Fig. 6a). The addition of catalysts leads to obvious degradation of RhB. CdS hollow spheres show much higher activity than that of commercial CdS and P25, and we also found that ZnS hollow spheres show impressive photocatalytic activity under UV-light illumination (Fig. 7). In addition to RhB, salicylic acid, a typical colorless contaminant was chosen as a goal organic pollutant which has no light absorption characteristics in the visible light region. Fig. 8 shows that CdS hollow spheres have high activity and salicylic acid can be decomposed efficiently in 6 h. The durability of CdS hollow spheres was tested by

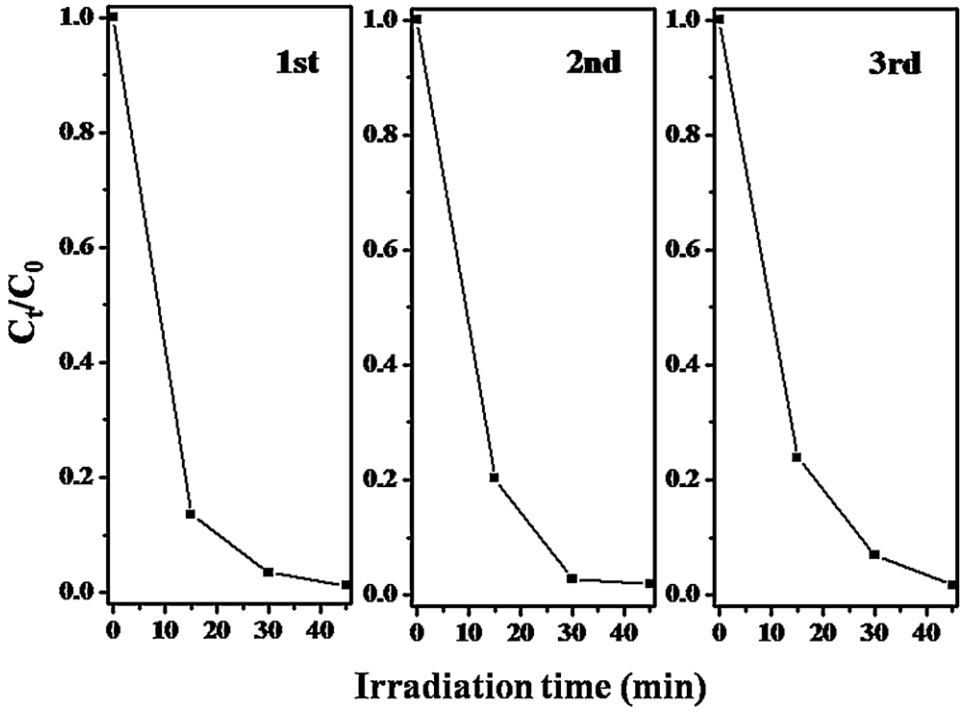

Fig. 9. Recycled photodegradation of RhB under the visible light (>420 nm) irradiation over CdS hollow spheres.

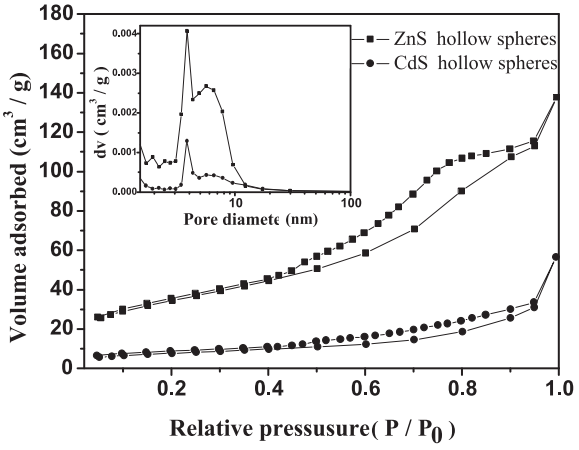

Fig. 10. Nitrogen adsorption–desorption isotherm and corresponding BJH pore-size distribution plot (inset) of CdS and ZnS hollow spheres.

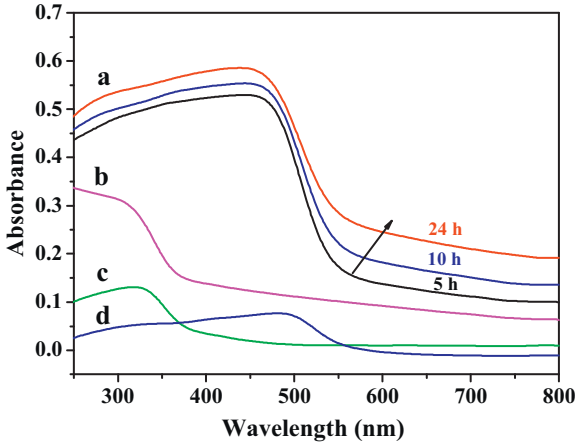

Fig. 11. UV–vis diffuse-reflectance spectra of (a) CdS hollow spheres samples obtained at 200 °C for 5 h, 10 h, 24 h, respectively, (b) ZnS hollow spheres (200 °C, 24 h), (c) commercial ZnS, (d) commercial CdS.

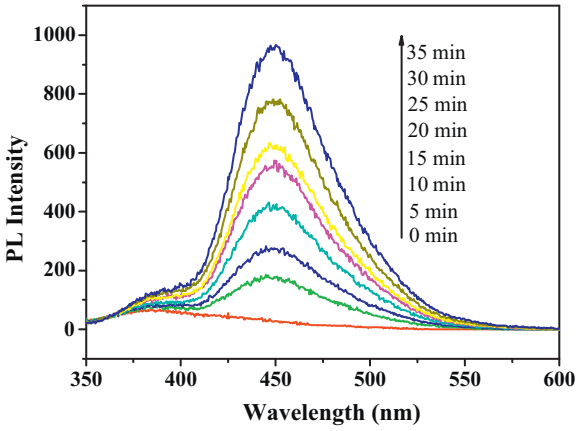

Fig. 12. PL spectra changes observed during visible light illumination (>420 nm) of CdS hollow spheres in coumarin solution (excitation at 332 nm).

RhB degradation for three recycles. As shown in Fig. 9, the catalyst can decompose RhB dye efficiently without significant deactivation after three times recycling. The corresponding XRD patterns (Fig. S3 in Supporting Information) have no notable differences of crystalline phase structure before and after the photocatalytic recycles except for the intensity. It indicates that the as prepared CdS hollow spheres are not photocorroded disastrously in the degradation of RhB.

The superiority of photocatalytic performance of the hollow CdS and ZnS samples is inferred to be a result of their special structural features. First, the rough surface of the hollow spheres provides high specific surface area and porosity. Fig. 10 shows the N_2 adsorption/desorption isotherm and the pore-size distribution (inset in Fig. 10) of the samples. The isotherms are identified as type IV, which indicates the mesoporosity of the shell walls of the hollow spheres. This finding is in good agreement with SEM and TEM observations. The pore-size distribution obtained from the isotherm reveals that the pores are less than 10 nm in diameter. These pores can promote rapid diffusion of the reactants and products during the photocatalytic reaction and thus enhance the rate of the photocatalytic reaction. The BET specific surface area and pore volume of the CdS hollow spheres were found to be 27.2 $m^2\ g^{-1}$ and 0.09 $cm^3\ g^{-1}$, which is lower than that of ZnS sample (123.0 $m^2\ g^{-1}$ and 0.21 $cm^3\ g^{-1}$). The lower BET surface area could be due to the thicker shell wall of CdS hollow spheres. In addition, the UV–vis diffuse-reflectance experiments reveal that the CdS hollow spheres samples have significantly enhanced light absorption in the visible region (400–550 nm) compared to bulk commercial CdS (Fig. 11). Similarly, the ZnS hollow spheres also have a stronger adsorption in the UV (200–400 nm) region than that of commercial ZnS. The enhanced light absorption can therefore provide more photocharges needed for the photocatalytic reactions.

For further insight into the photocatalytic mechanism and to study the involved active species in the photocatalytic process [38], the PL technique was employed to detect hydroxyl radicals (•OH) on the surface of visible light illuminated CdS spheres by using coumarin as a proble molecule [39] (see Scheme S1 in Supporting Information). Fig. 12 shows the changes in the PL spectra for 5×10^{-4} M coumarin solution with irradiation time in the presence of the CdS hollow spheres. It can be seen that a gradual increase in the PL intensity at about 445 nm is observed with increasing irradiation time. However, no PL intensity increase is observed in the absence of light irradiation or CdS hollow spheres indicating that the fluorescence is produced by chemical reactions of coumarin with •OH formed at the CdS–water interface via a photocatalytic reactions [40]. It is well known that the hydroxyl radical (•OH) is one of the major active species responsible for the photodegradation of organic molecules in the photcatalytic process and this result indicates that the fast production of •OH radicals and the highly accumulated •OH radicals may be the main active oxygen species in the photocatalytic process with the CdS hollow sphere system.

4. Conclusions

In summary, we have demonstrated a general one-pot strategy for synthesis of various metal sulfide hollow spheres, including CdS, ZnS, CuS, Bi_2S_3, etc. A possible growth mechanism was proposed to explain the formation of the hollow spheres self-assembled with single-crystal nanoparticles. Interestingly, the surface morphology and the shell thickness can be readily controlled by varying the ambient pressure and reaction time, respectively. These hollow spheres are promising for applications in the fields of catalysis, lithium-ion batteries, biomedicine and beyond. The research may open up new opportunities for preparing hollow structures for multipurpose applications.

Acknowledgements

The project was sponsored by the Scientific Research Foundation for the Returned Overseas Chinese Scholars, State Education Ministry (BZY09003) and Ministry of Human Resources and Social

Security (BZY09012). This work was also supported by National Natural Science Foundation of China (20803096, 21073238), the NSF of Hubei Province (Distinguished Young Investigator Grant 2010CDA082), Key Laboratory of Green Catalysis of Sichuan Institute of High Education (LYJ1108) and National Basic Research Program of China (Grant no. 2011CB211704).

Appendix A. Supplementary data

Supplementary data associated with this article can be found, in the online version, at http://dx.doi.org/10.1016/j.apcatb.2012.05.041.

References

[1] F. Caruso, R.A. Caruso, H. Mŏhwald, Science 282 (1998) 1111–1113.
[2] S.H. Im, U. Jeong, Y.N. Xia, Nature 4 (2005) 671–675.
[3] Y. Sun, Y.N. Xia, Science 13 (2002) 2176–2179.
[4] Y. Yin, Y.M. Robert, C.K. Erdonmez, S. Hughes, G.A. Somorjai, A.P. Alivisatos, Science 304 (2004) 711–714.
[5] J. Zhou, H. Song, X. Chen, L. Zhi, S. Yang, J. Huo, W. Yang, Chemistry of Materials 21 (2009) 2935–2940.
[6] M. Yang, J. Ma, C. Zhang, Z. Yang, Y. Lu, Angewandte Chemie International Edition 44 (2005) 6727–6730.
[7] X. Sun, S.A. Asher, Angewandte Chemie International Edition 43 (2004) 3827–3831.
[8] X. Xu, S.A. Asher, Journal of the American Chemical Society 126 (2004) 7940–7945.
[9] Y.F. Zhu, J.L. Shi, W.H. Shen, X.P. Dong, J.W. Feng, M.L. Ruan, Y.S. Li, Angewandte Chemie International Edition 44 (2005) 5083–5087.
[10] J. Liu, S.Z. Qiao, S.B. Hartono, G.Q. Lu, Angewandte Chemie International Edition 49 (2010) 4891–4895.
[11] X.W. Lou, Y. Wang, C. Yuan, J.Y. Lee, L.A. Archer, Advanced Materials 18 (2006) 2325–2329.
[12] X.W. Lou, L.A. Archer, Z.C. Yang, Advanced Materials 20 (2008) 3987–4019.
[13] A.M. Cao, J.S. Hu, H.P. Liang, L.J. Wan, Angewandte Chemie International Edition 44 (2005) 4391–4395.
[14] S.W. Kim, M. Kim, W.Y. Lee, T. Hyeon, Journal of the American Chemical Society 124 (2002) 7642–7643.
[15] J.G. Yu, X.X. Yu, Environmental Science and Technology 42 (2008) 4902–4907.
[16] S.H. Joo, J.K. Park, C.K. Tsung, Y. Yamada, P.D. Yang, G.A. Somorjai, Nature Materials 8 (2009) 126–131.
[17] Y.F. Zhu, D.H. Fan, W.Z. Shen, Langmuir 24 (2008) 11131–11136.
[18] X.B. Cao, L. Lu, L.G. Zhuge, W.J. Cao, W.C. Wang, S.F. Wu, Advanced Functional Materials 16 (2006) 896–902.
[19] Z.H. Dai, J. Zhang, J.C. Bao, X.H. Huang, X.Y. Mao, Journal of Materials Chemistry 17 (2007) 1087–1093.
[20] S. Ding, J.S. Chen, G. Qi, X. Duan, Z. Wang, E.P. Giannelis, L.A. Archer, X.W. Lou, Journal of the American Chemical Society 133 (2010) 21–23.
[21] H.P. Liang, H.M. Zhang, J.S. Hu, Y.G. Guo, L.J. Wan, C.L. Bai, Angewandte Chemie International Edition 43 (2004) 1540–1543.
[22] A.D. Dinsmore, M.F. Hsu, M.G. Nikolaides, M. Marquez, A.R. Bausch, D.A. Weitz, Science 298 (2002) 1006–1009.
[23] C.I. Zoldesi, A. Imhof, Advanced Materials 17 (2005) 924–928.
[24] D.H.M. Buchold, C. Feldmann, Nano Letters 17 (2007) 3489–3492.
[25] H. Zhou, T.X. Fan, D. Zhang, Q.X. Guo, H. Ogawa, Chemistry of Materials 19 (2007) 2144–2146.
[26] D. Walsh, B. Lebeau, S. Mann, Advanced Materials 11 (1999) 324–328.
[27] Y. Han, M. Fuji, D. Shchukin, H. Mŏhwald, M. Takahashi, Crystal Growth & Design 9 (2009) 3771–3775.
[28] Z. Yan, R. Bao, Y. Huang, D.B. Chrisey, Journal of Physical Chemistry C 114 (2010) 11370–11374.
[29] C. Wu, Y. Xie, L. Lei, S. Hu, C.Q. Yang, Advanced Materials 18 (2000) 1727–1732.
[30] J. Liu, D. Xue, Journal of Crystal Growth 311 (2009) 500–503.
[31] Z. Wu, K. Yu, S. Zhang, Y. Xie, Journal of Physical Chemistry C 112 (2008) 11307–11313.
[32] Q. Peng, Y.J. Dong, Y.D. Li, Angewandte Chemie International Edition 42 (2003) 3027–3030.
[33] B.P. Brinks, Current Opinion in Colloid and Interface Science 7 (2002) 21–41.
[34] C.J. Barrelet, Y. Wu, D.C. Bell, C.M. Lieber, Journal of the American Chemical Society 125 (2003) 11498–11499.
[35] C.E. Brennen, Cavitation and Bubble Dynamics, Oxford University Press, Oxford, UK, 1995.
[36] C.D. Ohl, O. Lindau, W. Lauterborn, Physical Review Letters 80 (1998) 393–396.
[37] Y. Zhao, L. Jiang, Advanced Materials 21 (2009) 3621–3638.
[38] T. Hirakawa, K. Yawata, Y. Nosaka, Applied Catalysis A-General 325 (2007) 105–111.
[39] H. Czili, A. Horvăth, Applied Catalysis B-Environmental 81 (2008) 295–302.
[40] C.S. Turch, D.F. Ollis, Journal of Catalysis 122 (1990) 178–192.